Short-Range Order and Site Connectivities in Sodium Aluminoborate Glasses: I. Quantification of Local Environments by High-Resolution ^{11}B, ^{23}Na, and ^{27}Al Solid-State NMR

Lars Züchner, Jerry C. C. Chan, Werner Müller-Warmuth, and Hellmut Eckert*

Institut für Physikalische Chemie, Westfälische Wilhelms-Universität Münster, Schlossplatz 7, D-48149 Münster, Germany

Received: December 29, 1997; In Final Form: March 12, 1998

The local structure of glasses in the system $Na_2O-B_2O_3-Al_2O_3$ is studied by multinuclear magic-angle spinning (MAS) solid-state NMR spectroscopy at 7.0 and 11.7 T. The ^{23}Na isotropic chemical shifts vary linearly with Na_2O concentration, indicating that the sodium ions are homogeneously distributed over the network and not clustered. The ^{11}B MAS NMR spectra reveal the presence of trigonal $BO_{3/2}$ units, tetrahedral $BO_{4/2}^-$ sites, and three-coordinate $BO_{2/2}O^-$ species containing nonbridging oxygen. The quantitative contributions of these three types of sites are obtained by detailed computer simulations of these spectra. High-resolution ^{27}Al satellite transition spectroscopy indicates that aluminum is predominantly present as $AlO_{4/2}^-$ sites. The structure of these glasses is discussed in terms of various melt reaction schemes, in which the network former oxides B_2O_3 and Al_2O_3 react with O^{2-} introduced by the network modifier Na_2O. While the data suggest that the formation of $AlO_{4/2}^-$ units takes priority over boron conversion, a detailed analysis of the oxide balance arising from these reactions indicates that small amounts of five- and six-coordinate aluminum must be present in nearly all of the samples; this conclusion is further confirmed by ^{27}Al 2-D triple-quantum NMR experiments. Although these high-resolution solid-state NMR spectra primarily inform about nearest-neighbor environments, they also allow inferences about the connectivities of these sites. Thus, a detailed inspection of compositional isotropic chemical shift trends suggests that the framework sites present in these glasses are not interlinked statistically, but rather that the tetrahedral $BO_{4/2}^-$ and $AlO_{4/2}^-$ sites are preferentially surrounded by three-coordinate boron. On the basis of this concept, it is also possible to explain the compositional dependence of the glass transition temperature on a structural basis in terms of an average framework site connectivity.

Introduction

Owing to their dielectric properties, their ionic conductivities, and their chemical resistivities, aluminoborate glasses are interesting candidates for a variety of industrial applications.[1,2] Wide glass-forming regions in the systems $Na_2O-Al_2O_3-B_2O_3$ and $CaO-Al_2O_3-B_2O_3$ allow tailoring of their physical and chemical properties to specifically desired applications.[3,4] To facilitate this process, it is important to develop a microscopic understanding of the structure and dynamics of glasses at the atomic level. In recent years, solid-state NMR spectroscopy has become one of the most important structural tools in glass science, providing intricate detail about the local environments present in the glassy state.[5,6] Borate glasses have attracted particular interest, because of the unusual effects of alkali and alkaline-earth oxides on their network structures.[5,7−13] Using ^{11}B wide-line NMR, it was shown that at low-to-moderate concentrations (0−33 mol %), these oxides increase the polymerization of the borate network, by converting symmetric trigonal $BO_{3/2}$ units into tetrahedral $BO_{4/2}^-$ - sites.[7−10] This finding provides a structural rationale for the experimentally observed stiffening of the glass structure as evidenced by increases of density, microhardness, and glass transition temperatures.[14−18] At higher oxide concentrations this effect is partially reversed, owing to the formation of asymmetric $BO_{2/2}O^-$ sites containing nonbridging oxygen species. Through systematic studies of many systems, quantitative structural models were developed, predicting the respective concentrations of $BO_{3/2}$, $BO_{4/2}^-$, and $BO_{2/2}O^-$ sites as a function of R, the alkali oxide/boron oxide molar ratio.[10−13] Adding aluminum oxide to an alkali or alkaline-earth borate glass has distinct effects on T_g, depending on the specific glass composition considered.[19,20] ^{11}B wide-line NMR studies indicate that at any given R value, the presence of aluminum reduces the fraction of four-coordinated boron atoms.[21−23] More recently, ^{27}Al MAS NMR spectra have revealed aluminum in four-, five-, and six-coordination with oxygen in these glasses.[23−26] The quantitative ratios of these species are composition-dependent and also affected by the cation type.[25,26] Whereas Al is predominantly four-coordinated in sodium aluminoborate glasses, larger amounts of such AlO_5 and AlO_6 units are found in the presence of highly polarizing cations such as Li^+ and Mg^{2+}. On the basis of bond valence concepts, Brow et al. estimate the stability of various oxygen nearest-neighbor environments in these glasses[27] and formulate rules for preferred and disfavored connectivities between various aluminum and boron sites. For instance, AlO_5 and AlO_6 polyhedra should be bonded to three- and four-coordinate oxygen, and $BO_{4/2}^--BO_{4/2}^--$ and $AlO_{4/2}^--AlO_{4/2}^-$ connectivities are predicted to be less stable than $BO_{3/2}-AlO_{4/2}^-$ connectivities. Figure 1 shows the glass-forming region of the sodium aluminoborate glass system. We have conducted a

S1089-5647(98)00587-2 CCC: $15.00
Published on Web 05/19/1998

detailed quantitative structural study, the results of which will be presented in two parts. Part I (this contribution) focuses on the detailed identification and quantification of the various distinct boron and aluminum sites present in these glasses. Field-dependent MAS NMR, satellite transition, and triple quantum NMR spectroscopies have been used to extract average values of nuclear electric quadrupolar coupling constants and isotropic chemical shift values for the quadrupolar nuclei ^{11}B, ^{23}Na, and ^{27}Al. On the basis of the compositional dependences of the site speciations and NMR Hamiltonian parameters, inferences can be made on preferred connectivities. In part II, these inferences and the predictions by Brow et al. are tested quantitatively by measuring internuclear dipole−dipole couplings via double-resonance NMR techniques. The detailed structural model for sodium aluminoborate glasses emerging from both studies will be discussed in relation to the structural findings of other aluminum-containing glass systems.

NMR Methodology

In general, the quadrupolar interactions of the nuclei ^{11}B ($I = {}^3/_2$), ^{23}Na ($I = {}^3/_2$), and ^{27}Al ($I = {}^5/_2$) in inorganic compounds are moderately strong, so that the $\Delta m = \pm 1$ transitions are anisotropically split and broadened over a frequency range of several megahertz.[28] In these cases the analysis focuses on the central $m = {}^1/_2 \leftrightarrow m = -{}^1/_2$ transition. To calculate the corresponding NMR powder line shape in these cases, second-order perturbation theory is required. The complex angular dependence of the central transition energy results in only incomplete line-narrowing by magic-angle spinning.[29] Partially narrowed, structured MAS NMR line shapes are observed, from which isotropic chemical shifts and nuclear electric quadrupolar coupling parameters can be extracted in principle.[29] As previously shown, simulation of ^{11}B NMR spectra using single-valued Hamiltonian parameters can reproduce the experimentally observed line shapes in glasses reasonably well, albeit not exactly.[30] The approach is even grossly inadequate for ^{27}Al and ^{23}Na MAS NMR spectra in glasses. Here, it is necessary to assume wide distributions of chemical shifts and quadrupolar couplings, reflecting continuous local variations in the bond lengths and bond angles. Despite this complication, average Hamiltonian parameters can be extracted from field-dependent NMR spectra. From the center of gravity a resonance shift δ_{exp} is observed, which is the sum of the isotropic chemical shift and the second-order quadrupolar shift[31]

$$\delta_{exp} = \delta_{iso} + \delta_{QS}^{(2)}$$

where

$$\delta_{QS}^{(2)} = -\frac{3}{40}\frac{\chi^2}{\nu_0^2}\frac{I(I+1) - 9m(m-1) - 3}{I^2(2I-1)^2} \qquad (1)$$

In this expression, ν_0 is the Larmor frequency while

$$\chi = C_Q\left(1 + \frac{\eta^2}{3}\right)^{1/2} \qquad (2)$$

where C_Q is the principal component and η is the asymmetry parameter of the nuclear electric quadrupolar interaction tensor. By comparison of the centers of gravity at both field strengths, it is possible to obtain δ_{iso} and χ.

One aspect important for the present study is the fact that for $I = {}^5/_2$ nuclei the second-order quadrupolar shift (and also the anisotropic broadening of the MAS NMR line shape) of adjacent $|m| = {}^1/_2 \leftrightarrow |m| = {}^3/_2$ "satellite" transitions is substantially smaller than that of the central transition.[32] Thus, the resolution in MAS NMR is substantially increased by observing the sideband manifold associated with these satellite transitions.[33] While these benefits have been previously demonstrated also for a variety of glassy samples,[34−36] systematic applications of this method for structural studies of glasses have appeared only recently.[37,38] The second aspect of relevance relates to the fact that the $m = -{}^3/_2 \leftrightarrow m = +{}^3/_2$ triple-quantum transition, albeit forbidden, has no intrinsic anisotropy arising from the first-order quadrupolar coupling.[39] This feature has been exploited recently for recording high-resolution solid-state NMR spectra of quadrupolar nuclei with standard solid-state NMR instrumentation.[40−44] The pulse sequence is shown in Figure 2. In essence, the first pulse excites triple-quantum coherence, which is allowed to evolve for the duration of the evolution time t_1. The evolution is then stopped by the second pulse. The third pulse (generally applied at a lower radio-frequency power level) produces single quantum coherence, corresponding to observable magnetization. Incrementation of t_1 and subsequent 2-D data processing allows the regular MAS NMR spectrum (dominated by quadrupolar broadening) to be correlated with a spectrum that is solely governed by isotropic quadrupolar and chemical shifts. In the present study, both satellite transition spectroscopy and 2-D triple-quantum MAS NMR have been used to extract accurate ^{27}Al chemical shift

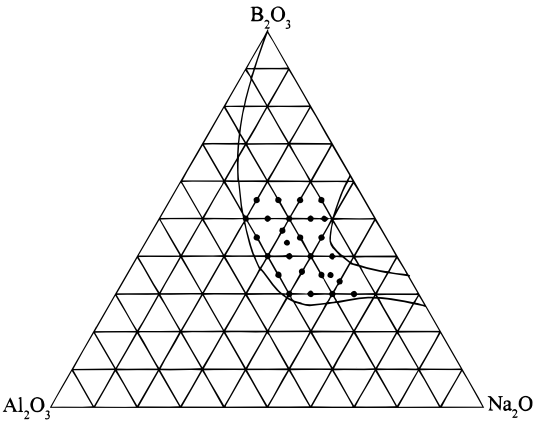

Figure 1. Compositional diagram, indicating the region of glass formation in the glass system $B_2O_3-Al_2O_3-Na_2O$. After Imaoka, M. *Rep. Inst. Ind. Sci.* **1957**, *6*, 144. The samples investigated in the present study are indicated.

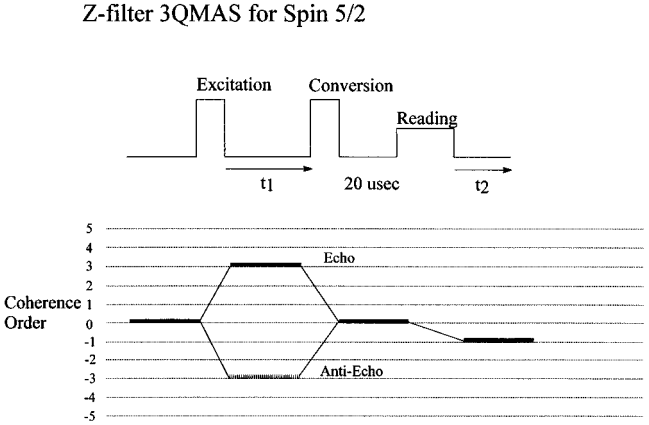

Figure 2. Pulse sequence and coherence level diagram used for recording the ^{27}Al 3Q MAS NMR spectra of the present study.

TABLE 1: Compositions and Glass Transition Temperatures of the Glasses under Study

sample no.	mol % Na_2O	mol % B_2O_3	mol % Al_2O_3	T_g/°C ± 5
1	20	55	25	456
2	20	50	30	484
3	25	55	20	448
4	25	50	25	439
5	25	45	30	449
6	30	55	15	435
7	30	50	20	432
8	30	47	23	424
9	30	40	30	446
10	33	44	24	407
11	35	55	10	428
12	35	50	15	412
13	35	45	20	410
14	35	40	25	404
15	35	35	30	399
16	38	50	12	401
17	40	45	15	386
18	40	40	20	376
19	40	36	24	369
20	40	30	30	372
21	45	40	15	362
22	45	35	20	356
23	45	30	25	370
24	47	35	18	352
25	50	33	17	330
26	50	30	20	320
27	55	30	15	307

information for the various aluminum environments present in sodium aluminoborate glasses.

Experimental Section

Sample Preparation and Characterization. Figure 1 and Table 1 summarize the batch compositions of the sodium aluminoborate samples under study. Na_2CO_3 (99%, Fluka), B_2O_3 (99% Merck), and Al_2O_3 (99%, Merck) were ground together and melted for 20−30 min in an induction furnace using a Pt crucible. The samples were quenched to room temperature by pouring the melt onto a water-cooled block of copper, resulting in optically clear materials with no apparent inhomogeneities. Batch and sample weights were carefully recorded on representative samples, indicating that evaporation losses were below 3%. Therefore, sample compositions were assumed to be identical to batch compositions for all of the samples investigated. The formation of entirely glassy materials was ascertained by the absence of any sharp X-ray powder diffraction peaks (Seiffert & Co. diffractometer, Cu K_α line). Glass transition temperatures were measured using a NETZSCH differential scanning calorimeter (heating rate 10 °C/min) and are included in Table 1. All of the samples showed single thermal events, consistent with the formation of homogeneous single-phase materials.

Nuclear Magnetic Resonance Studies. Solid-state NMR experiments were carried out on Bruker spectrometers DSX-Avance 500 and CXP-300 (with TECMAG pulse programmer and data system) using 4 mm high-speed spinning probes. At the two field strengths of 7.05 and 11.74 T, the resonance frequencies were, respectively, 96.3 and 160.5 MHz for ^{11}B, 78.2 and 130.3 MHz for ^{27}Al, and 79.4 and 132.3 MHz for ^{23}Na. Typical acquisition parameters were spinning speed 13.5 kHz, pulse length 1 μs, recycle delay 1s (^{23}Na, ^{27}Al) and 5s (^{11}B), respectively, 500 scans. Isotropic chemical shifts are reported with respect to $BF_3 \cdot Et_2O$, 1 M $AlCl_3$, and 1 M NaCl solutions, respectively. The nutation behavior for all of the nuclei was carefully characterized, and pulse lengths were chosen such that flip angles were sufficiently short to ensure representative results even in cases where species with different nutation behaviors were observed. For the ^{27}Al nuclei, more accurate isotropic chemical shift information was sought from the MAS sideband patterns belonging to the $|m| = {}^1/_2 \leftrightarrow |m| = {}^3/_2$ satellite transitions. These "SATRAS" spectra were recorded using pulse lengths of 0.6 μs and 100 000 scans. All the ^{27}Al 3QMAS spectra were obtained at a spinning rate of 12 kHz by the *z*-filtering sequence.[45] The RF field strengths of the first two hard pulses and the third soft pulse corresponded to nutation frequencies of approximately 135 and 6 kHz, respectively, for a liquid sample. The optimized pulse widths were determined to be 3.0, 1.0, and 12.5 μs for the three consecutive pulses. A 72-step phase cycle was employed to select the 3Q coherences and cancel all transverse magnetization after the second hard pulse. Typically 576 transients were accumulated for each t_1 increment, and a total of 64 increments were done at steps of 5 μs. A relaxation delay of 0.2 s was employed. Quadrature detection in the F_1 dimension was achieved by the hypercomplex approach.[46] The sheared spectra were analyzed by projecting each individual site onto the F_1 and F_2 axes.[47]

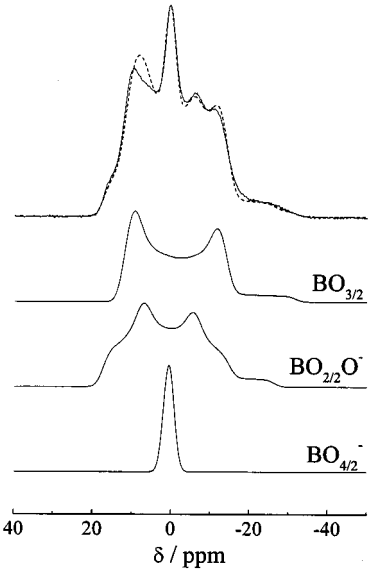

Figure 3. Experimental and simulated ^{11}B MAS NMR spectra of a typical sodium aluminoborate glass (no. 19). Individual spectral components are shown.

Results and Interpretation

1. Spectral Deconvolution and Simulations. Figure 3 shows a representative 7.05 T ^{11}B MAS NMR spectrum for a glass containing 40 mol % Na_2O, 36 mol % B_2O_3, and 24 mol % Al_2O_3. Included is a simulation showing the spectral contributions of $BO_{4/2}^-$, $BO_{3/2}$, and $BO_{2/2}O^-$ sites. Table 2 summarizes, for all of the glasses, the respective fractions N_4, N_3, and N_2 of these boron sites and their ^{11}B spectroscopic parameters as deduced from the field-dependent measurements using eqs 1 and 2. The fit parameters used in the simulations were varied manually to accomplish acceptable fits to the experimental spectra at both field strengths. For two glasses (25, 27) the spectra indicate the presence of moderate amounts of pyroborate ($BO_{1/2}O_{-2}$) groups; their respective fractions, N_1, and their ^{11}B NMR Hamiltonian parameters are included in Table 2. The presence of these units is quite plausible in these high-sodium glasses. Figure 4 shows typical results for a few glasses. The $BO_{4/2}^-$ resonance has an approximately Gaussian

TABLE 2: ^{11}B NMR Parameters of the Glasses under Study[a]

	$BO_{3/2}$ sites				$BO_{2/2}O^-$ sites				$BO_{4/2}^-$ sites		
sample no.	N_3/% ± 10	δ_{iso}/ppm ± 0.6	C_Q/MHz ± 0.05	η ± 0.10	N_2 (N_1)/% ± 10	δ_{iso}/ppm ± 0.6	C_Q/MHz ± 0.05	η ± 0.10	N_4/% ± 4	δ_{iso}/ppm ± 0.2	χ/kHz ± 50
1	92.5	17.3	2.63	0.28					7.5	1.3	594
2	95.8	17.4	2.68	0.23					4.3	0.8	502
3	76.5	18.0	2.66	0.23					23.5	1.1	527
4	88.3	17.4	2.66	0.15					11.8	1.0	476
5	94.8	17.3	2.68	0.15					5.3	1.0	502
6	70.5	18.2	2.64	0.15					29.5	1.2	527
7	72.8	18.1	2.65	0.20					27.3	1.0	550
8	84.0	18.3	2.71	0.15					16.0	1.1	541
9	94.8	17.7	2.71	0.00					5.3	0.9	550
10	68.5	18.0	2.70	0.15	15.0	19.2	2.58	0.30	16.5	1.5	635
11	49.0	18.4	2.68	0.20	19.3	19.8	2.56	0.30	31.8	1.7	692
12	49.5	18.1	2.69	0.18	24.5	19.6	2.56	0.30	26.0	1.4	594
13	60.5	18.3	2.70	0.18	17.0	19.0	2.58	0.30	22.5	1.3	573
14	65.0	17.9	2.72	0.05	20.8	19.2	2.58	0.28	14.3	1.4	615
15	76.0	17.9	2.72	0.00	18.8	19.5	2.56	0.33	5.3	1.3	655
16	43.0	17.8	2.70	0.18	32.3	19.4	2.56	0.30	24.8	1.3	573
17	30.0	17.9	2.70	0.15	48.5	19.6	2.56	0.35	21.5	1.4	573
18	40.0	17.8	2.72	0.05	45.0	19.7	2.58	0.33	15.0	1.5	615
19	39.0	18.0	2.72	0.05	51.3	19.5	2.58	0.40	9.8	1.4	573
20	56.0	18.2	2.72	0.03	40.0	19.5	2.60	0.40	4.0	1.6	635
21	16.0	17.9	2.74	0.05	69.8	19.4	2.56	0.40	14.3	1.2	420
22	25.0	17.8	2.72	0.08	66.8	19.6	2.58	0.38	8.3	1.7	655
23	29.5	17.7	2.72	0.00	64.5	19.8	2.59	0.36	6.0	1.6	655
24	12.0	17.5	2.72	0.03	78.8	19.7	2.59	0.40	9.3	1.8	635
25					76.5 (12.5)	19.5 (19.6)	2.58 (2.58)	0.48 (0.15)	11.0	1.7	573
26	10.0	18.7	2.73	0.13	86.0	19.8	2.59	0.41	4.0	1.6	527
27					71.3 (22.5)	19.8 (20.0)	2.55 (2.55)	0.50 (0.2)	6.3	1.6	502

[a] Numbers in brackets refer to pyroborate ($BO_{1/2}(O^-)_2$) sites.

line shape, reflecting dipolar interactions, whereas the quadrupole coupling is weak ($\chi \approx 500-700$ kHz) in agreement with the local symmetry. The three-coordinated boron sites show strong second-order quadrupolar effects on the ^{11}B MAS NMR line shapes. As Table 2 illustrates, the interaction parameters of the $BO_{3/2}$ and the $BO_{2/2}O^-$ groups are also quite distinct from each other but show fairly consistent values from sample to sample. For the $BO_{2/2}O^-$ sites the absence of D_{3h} symmetry manifests itself in a large asymmetry parameter of the quadrupolar interaction tensor. At 11.7 T the $BO_{4/2}^-$ resonance is well-separated from the trigonal boron resonances; on the other hand, the 7.0 T spectra facilitate the spectral deconvolution into $BO_{3/2}$ and $BO_{2/2}O^-$ sites. The most important, albeit minor, disagreement between the experimental spectra and the simulations is the intensity ratio of the two singularities associated with the resonance of the $BO_{3/2}$ groups. This effect reveals that assuming singular values of nuclear electric quadrupolar coupling constants for these spectra is too simple and that a distribution function would be more appropriate.

Figures 5 and 6 show typical ^{27}Al and ^{23}Na MAS NMR spectra and the dependence of δ_{iso} on composition. For both nuclei, the asymmetrically broadened resonances (which become narrower at higher field strengths) are symptomatic of strong second-order quadrupolar effects with wide distributions of electric field gradients. Average values of χ and δ_{iso}, deduced from field-dependent measurements of the centers of gravity of the ^{23}Na central transition spectra, are included in Table 3. Figure 7 shows ^{27}Al magic-angle spinning sideband manifolds associated with the first satellite transitions. With the exception of a few samples, these MAS NMR data suggest the exclusive presence of tetrahedrally coordinated $AlO_{4/2}^-$ sites. Approximate ^{27}Al χ and δ_{iso} values obtained from these SATRAS spectra are listed in Table 3. For selected samples, values measured independently by triple-quantum NMR have been included for comparison. While the isotropic chemical shifts determined by both methods are generally in reasonable agreement (and yield the same compositional trends), the corresponding χ values show minor systematic deviations in both methods. One possible source of error is the extremely wide distribution of nuclear electric quadrupolar coupling constants that is particularly evident in the slices along the anisotropic dimensions of the 2-D triple-quantum spectra. As a result of this wide distribution it is possible that the weighing of the different spectral contributions to average χ values is different by both methods. From the 2-D triple-quantum spectra important additional information about the site speciation of aluminum is available. As exemplified by Figure 8, the 2-D contours reveal small amounts of five- and six-coordinate aluminum species for most of the samples. These species are not apparent in the one-dimensional MAS NMR spectra of either the central or the satellite transitions because of the much more limited spectroscopic resolution available. Because of overlap with spinning sideband artifacts they are also not clearly visible in the projections of the 2-D spectra onto the isotropic frequency axis. The results obtained here demonstrate nicely the benefits of the two-dimensional aspects of the triple-quantum experiment in documenting the presence of higher-coordinated aluminum. Although these experiments do not lend themselves easily to quantitative studies, we estimate that, with the exception of samples 1, 2, and 5, the respective fractions of five- and six-coordinate aluminum are below 5%. Table 4 summarizes the interaction parameters for the five- and six-coordinated aluminum sites, measured by triple-quantum NMR. In addition, quantitative estimates are included, which in glasses 1, 2, and 5 are obtained from an analysis of the SATRAS spectra. For the other glasses, estimates of the combined fractions $N_{5,6}$ of higher-coordinated aluminum are deduced from oxide balance considerations (see below).

Compositional Dependence of NMR Parameters. Examination of the ^{11}B, ^{27}Al, and ^{23}Na NMR data summarized in

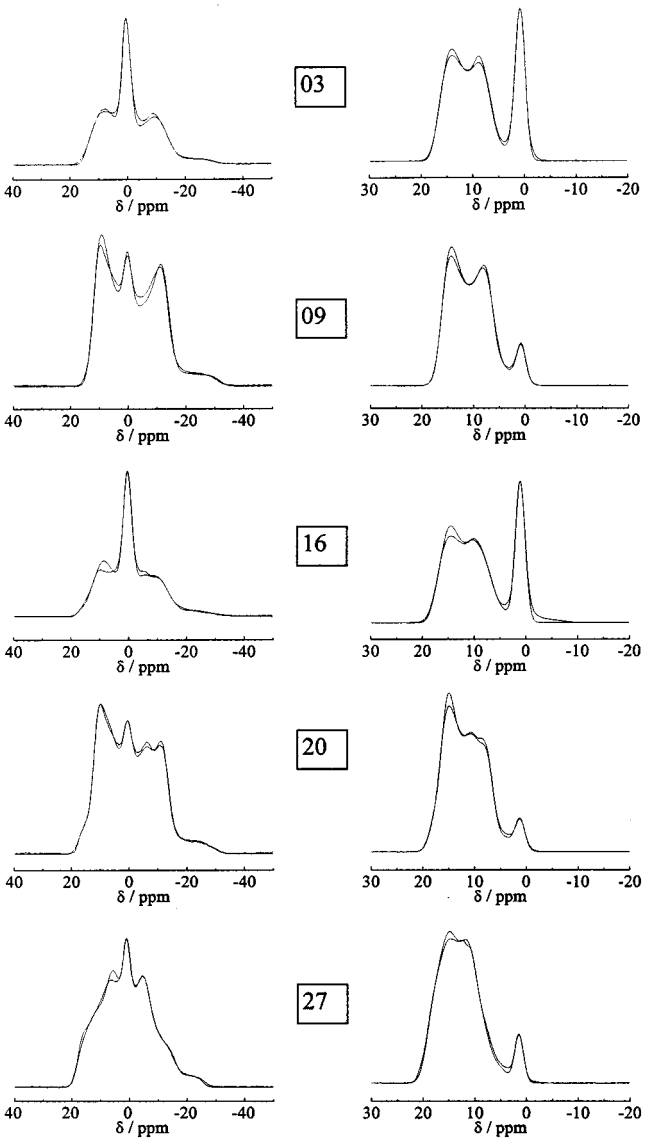

Figure 4. Field-dependent experimental and simulated ^{11}B MAS NMR spectra of representative sodium aluminoborate glasses. Left side, spectra at 7.04 T (96.2 MHz); right side, spectra at 11.74 T (160.3 MHz).

Tables 2−4 for the individual sites reveal certain systematic dependences on the elemental composition. The ^{23}Na isotropic shifts and the ^{27}Al isotropic shifts of the $AlO_{4/2}^-$ units reveal excellent linear correlations with the Na_2O content. A similar correlation appears to be present for the AlO_5 units but not for the AlO_6 sites. Furthermore, Figure 9 shows that the ^{11}B isotropic chemical shifts of the framework groupings $BO_{4/2}^-$ are also linearly correlated with the sodium concentration, whereas the isotropic chemical shifts of the framework groupings $BO_{3/2}$ and $BO_{2/2}O^-$ are independent of this parameter. The nuclear electric quadrupolar coupling parameters of ^{11}B, ^{23}Na, and ^{27}Al show no systematic compositional trends.

Discussion

Competing Network Conversion Reactions. It has become customary in glass science to account for the formation of the various coordination environments present in glasses by postulating melt reaction schemes. In these schemes, the framework sites arising from the network former oxides B_2O_3 and Al_2O_3 react with the O^{2-} ions introduced by the network modifying

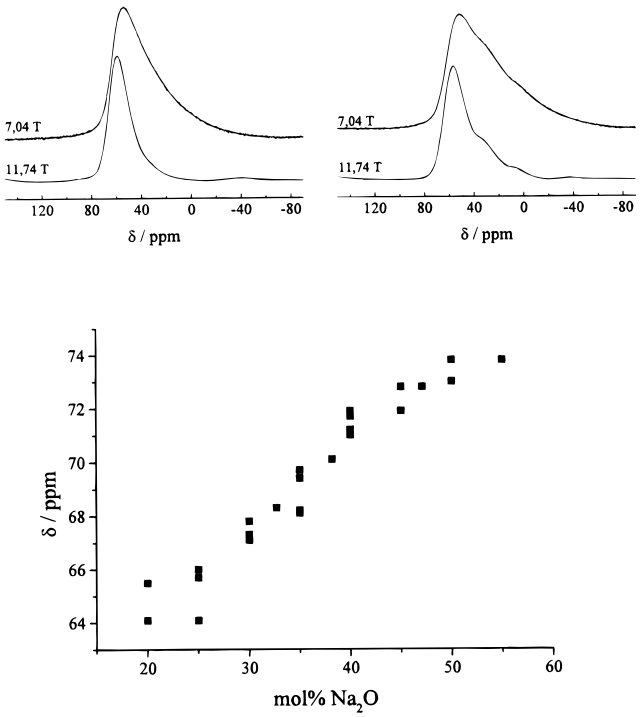

Figure 5. ^{27}Al MAS NMR results on sodium aluminoborate glasses. Top: Representative field-dependent spectra of two glass compositions. Left side, glass no. 7; right side, glass no. 2. Bottom: Dependence of the isotropic chemical shift of the dominant $AlO_{4/2}^-$ line on sodium oxide concentration.

oxides. For sodium aluminoborate glasses, the following reactions have been postulated:

$$2AlO_{6/4} + O^{2-} \rightarrow 2AlO_{4/2}^- \quad \text{(A)}$$

$$2BO_{3/2} + O^{2-} \rightarrow 2BO_{4/2}^- \quad \text{(B)}$$

$$2BO_{3/2} + O^{2-} \rightarrow 2BO_{2/2}O^- \quad \text{(C)}$$

In the present glass system, Na^+ is the predominant counterion, while eq. A shows aluminum in the role of a network former species. However, it has been pointed out that aluminum can principally also serve as a network modifier, for example, according to the reaction

$$4AlO_{6/4} \rightarrow Al^{3+} + 3AlO_{4/2}^- \quad \text{(D)}$$

The Al^{3+} produced in this fashion is assumed to be six-coordinated. If it is proximal to the anionic tetrahedral aluminum sites, one also speaks of "triclusters".[48]

Previous NMR results have shown that in sodium and calcium aluminoborate glasses with fixed R = (mol % $M_{(2)}O$)/(mol % B_2O_3), the fraction of tetrahedrally coordinated boron atoms is reduced successively when an increasing amount of aluminum oxide is added. On the basis of this finding, it was suggested that reaction A takes priority, while the extent to which reactions B and C proceed is limited by the amount of Na_2O still available after subtracting that consumed in reaction A.[21] Indeed, the ^{27}Al MAS NMR spectra show that the overwhelming fraction of aluminum is four-coordinated, suggesting that this model is broadly correct. Still, inspection of the oxide balance (see below) indicates the need for refinement. For example, considering the ^{11}B MAS spectra of glasses with Al/Na ratios ≥ 1, moderate amounts of tetrahedral boron are evident. In

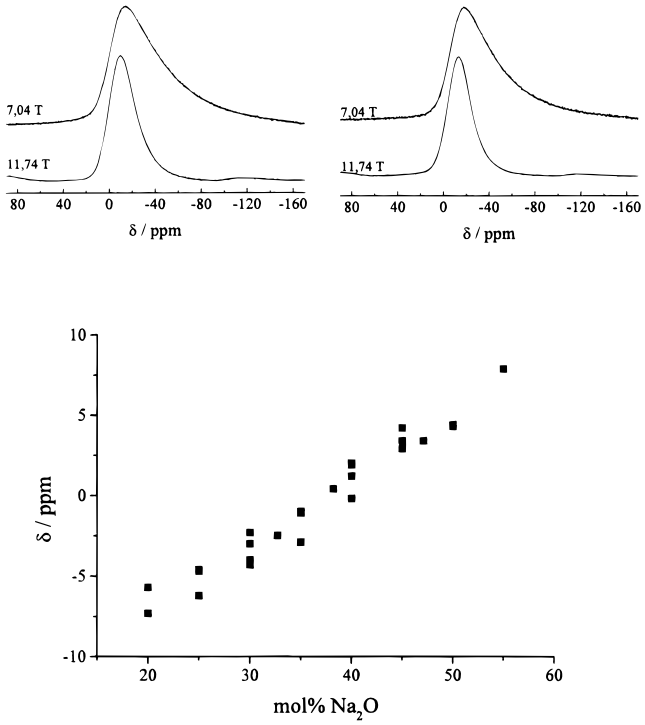

Figure 6. ^{23}Na MAS NMR results on sodium aluminoborate glasses. Top: Representative field-dependent spectra of two glass compositions. Left side, glass no. 7; right side, glass no. 2. Bottom: Dependence of the isotropic chemical shift on sodium oxide concentration.

TABLE 3: Average ^{23}Na and ^{27}Al Isotropic Chemical Shifts (Tetrahedral $AlO_{4/2}^-$ Sites Only) and Nuclear Electric Quadrupolar Coupling Constants in the Glasses Studied[a]

sample	^{23}Na		^{27}Al	
no.	δ_{iso}/ppm ± 1.0	χ/MHz ± 0.1	δ_{iso}/ppm ± 1.0	χ/MHz ± 0.3
1	−7.3	2.35	64.1	5.4
2	−5.7	2.38	65.5 (63.9)	5.5 (4.3)
3	−4.7	2.50	65.7 (64.3)	5.2 (4.1)
4	−6.2	2.23	64.1	4.9
5	−4.6	2.37	66.0	5.3
6	−3.0	2.48	67.2 (65.6)	5.4 (4.1)
7	−4.0	2.34	67.1 (66.0)	5.2 (4.3)
8	−2.3	2.47	67.8	5.5
9	−4.3	2.22	67.3 (65.3)	5.4 (4.2)
10	−2.5	2.41	68.3	5.6
11	−2.9	2.36	68.2 (66.2)	5.6 (4.3)
12	−1.1	2.46	68.1	5.5
13	−1.0	2.57	68.1	5.5
14	−1.0	2.49	69.4	5.7
15	−1.0	2.43	69.7 (67.7)	5.7 (4.4)
16	0.4	2.48	70.1 (67.6)	5.8 (4.0)
17	1.2	2.48	71.0	5.8
18	−0.2	2.28	71.2 (69.5)	5.8 (4.3)
19	2.0	2.44	71.7	5.7
20	1.9	2.48	71.9 (71.6)	5.9 (4.7)
21	3.4	2.48	71.9	5.6
22	2.9	2.36	72.8	5.7
23	4.2	2.55	72.8 (72.4)	5.8 (4.9)
24	3.4	2.31	72.8	5.6
25	4.3	2.34	73.0 (72.2)	5.4 (4.5)
26	4.4	2.30	73.8	5.5
27	7.9	2.55	73.8 (73.0)	5.5 (4.4)

[a] Numbers in parentheses were determined from analysis of 3Q-MAS NMR spectra.

contrast, the "aluminum priority" model would predict $N_4 = 0$, owing to lack of Na_2O availability for reaction B.

Oxide Balance and Higher-Coordinated Aluminum. Assuming the glass formation to be governed by reactions A−C,

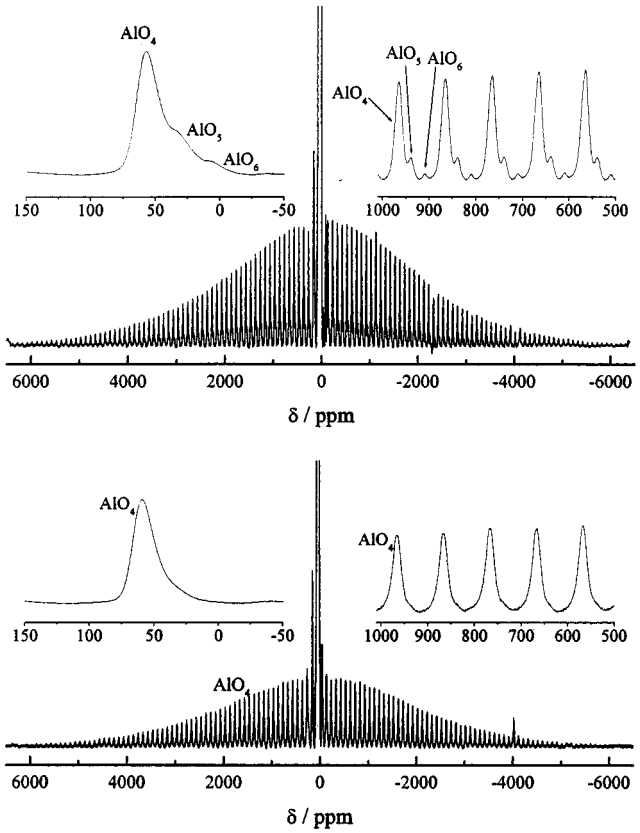

Figure 7. ^{27}Al central and satellite transition spectra of two representative glass compositions: glass 2 (top) and glass 11 (bottom). The complete spectra with the sidebands are shown together with the central resonance (top left) and five selected sidebands (top right) on an expanded scale.

it is possible to back-calculate an expected molar concentration of Na_2O for each glass, using the fractions of $BO_{4/2}^-$ and $BO_{2/2}O^-$ units from the ^{11}B MAS line shape simulations and assuming that all of the aluminum is present as $AlO_{4/2}^-$ sites.

Figure 10 illustrates that this theoretically expected Na_2O concentration is indeed closely correlated with the actual sodium oxide batch content, indicating that the "aluminium priority model" is realistic to a first approximation. Nevertheless, in nearly all of the cases, the back-calculated Na_2O contents are somewhat higher than those actually present. Naturally, the largest discrepancies are found for glasses with Al/Na ratios > 1 (samples 1, 2, and 5), where aluminum conversion cannot exclusively proceed by reaction A.

The discrepancy evident in Figure 10 can be remedied by assuming that not all of the aluminum is present as $AlO_{4/2}^-$ sites. Indeed, five- and six-coordinate aluminum species are clearly evident in the magic-angle spinning NMR spectra of glasses 1, 2, and 5, and further, the 3Q-MAS NMR spectra of nearly all of the other glasses investigated reveal the presence of higher-coordinated aluminum species. It is possible to estimate the fraction of aluminum present in a higher-coordinated state by taking into account the stoichiometries of reactions A−C and the experimental concentrations of $BO_{4/2}^-$ and $BO_{2/2}O^-$ units. One conceivable scenario would assign all aluminum left over after accounting for reactions A−C to a higher-coordinated state. This scenario results in unrealistically high AlO_5 and AlO_6 site concentrations inconsistent with the SATRAS data. On the other hand, we can give a lower limit on the fraction of higher coordinate aluminum by assigning all leftover aluminum to reaction D. The estimated fractions $N_{5,6}$ are included in Table 4 and found to be much more consistent

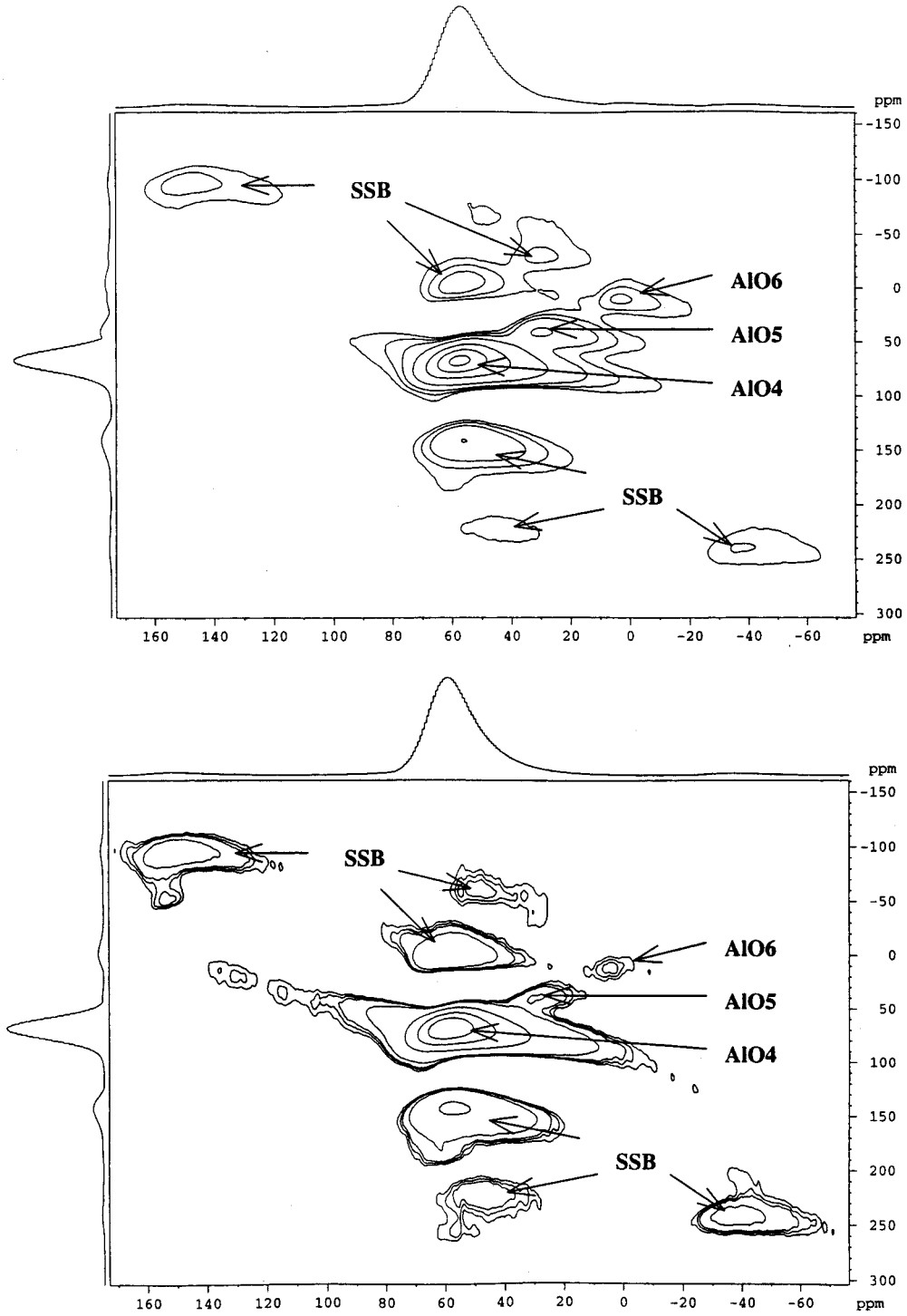

Figure 8. Typical ^{27}Al 3QMAS spectra of two sodium aluminoborate glasses at 11.74 T. Glass 2 (top) and glass 7 (bottom). Spectroscopic features typical of five- and six-coordinate aluminum are specifically indicated. Spinning sideband artifacts are marked "SSB".

with the AlO_5 and AlO_6 site concentrations measured by SATRAS for glasses 1, 2, and 5. As a caveat, we note that owing to the experimental error (estimated conservatively at $\pm 10\%$) of the boron speciation results, the inferred percentages of higher-coordinated aluminum still contain zero within their error limits for many of the glass samples studied here. Nevertheless, the consistency of the effect as well as the 3Q-MAS results provide strong evidence for small amounts of higher-coordinated aluminum in many sodium aluminoborate glasses studied here.

It is interesting to compare the aluminum speciations obtained for sodium aluminoborate glasses with those known for other glass systems. The predominance of four-coordinated aluminum is also a common feature in aluminosilicate glasses, as recently illustrated by SATRAS results on the system $K_2O-SiO_2-Al_2O_3$.[37] Both glass systems have in common that the concentrations of higher-coordinated aluminum are particularly large in samples with alumina/alkali oxide molar ratios exceeding one.[37] In contrast, generally much larger amounts of five- and six-coordinate aluminum sites are observed in calcium aluminoborate glasses,[25] aluminophosphate glasses,[49] and the glass system $Al_2O_3-B_2O_3-P_2O_5$.[38]

Inferences of Preferred Framework Site Connectivities. It is important to realize that the quantitative site speciation

TABLE 4: ^{27}Al NMR Parameters of Five- and Six-Coordinated Aluminum Sites, As Extracted from SATRAS Spectra[a]

	AlO_5			AlO_6			
	δ_{iso}/ppm ± 1	χ/MHz ± 0.6	N_{5Al}/% ± 5	δ_{iso}/ppm ± 1	χ/MHz ± 0.6	N_{6Al}/% ± 5	$N_{5,6}$/%
1	36.6	4.0	6	–	–	<1	9 ± 2
2	38.3 (37.1)	3.9 (4.6)	2	9.3 (8.0)	2.8 (3.6)	13	10 ± 2
3	(38.1)	(4.6)		(14)	(3.0)		10 ± 3
4							6 ± 2
5	–	–	–	13.2	–	3	6 ± 2
6	(36.5)	(4.4)		(8.4)	(4.1)		2 ± 4
7	(38)	(4.5)		(9.6)	(3.8)		5 ± 2
8							1 ± 2
9	–	–	–	(15.3)	(3.8)		2 ± 1
10							5 ± 6
11	(36.5)	(4.4)		–	–	–	8 ± 17
12							9 ± 12
13							4 ± 7
14							4 ± 5
15	–	–		(9.6)	(3.7)		3 ± 4
16	(40.6)	(3.8)		(7.7)	(3.0)		5 ± 14
17							11 ± 11
18	(41.6)	(3.9)		(10.1)	(3.1)		5 ± 7
19							6 ± 5
20	–	–	–	(12)	(3.1)		3 ± 3
21							6 ± 9
22							2 ± 6
23							1 ± 4
24							3 ± 7
25	(44.7)	(3.8)		(14.6)	(3.5)		6 ± 6
26							0 ± 2
27	(44.5)	(4.4)		(12.9)	(2.9)		0 ± 1

[a] Data in parentheses are extracted from 3 Q-MAS data. Dashed entries indicate that 3Q-MAS was attempted but S/N was too small to detect the species without doubt. Absence of an entry indicates that higher coordinated Al was not detected by SATRAS and glasses were not studied by 3Q-MAS. The quantity $N_{5,6}$ denotes the fraction of higher-coordinated Al sites as deduced from oxide balance considerations (see text). Specified errors arise from the intrinsic error in the analysis of the ^{11}B MAS spectra (see text).

afforded by MAS peak deconvolution is only a first step in the structural analysis of a glass. For a more detailed understanding, it is important to elucidate the connectivity, i.e., the question of how specific framework species are linked in establishing the overall network. Is the linking purely statistical, or do preferred site connectivities exist? This issue will be addressed in more detail in part II of this study, using specific dipolar NMR approaches. Nevertheless, indirect evidences for preferred framework site connectivities in sodium aluminoborate glasses are also available from the data obtained in the present study. One piece of information comes from a detailed analysis of the boron conversion process. As is well-known from NMR spectra of binary alkali borate glasses, network conversion can proceed by the competing reactions B and C. For low alkali contents ($R \leq 0.5$), reaction B dominates, while for $R > 0.5$, the formation of three-coordinate $BO_{2/2}O^-$ species is increasingly favored. The competition between both reactions can be expressed by the ratio N_2/N_4, which is plotted in Figure 11 as a function of R. Here, the data for the present sodium aluminoborate glasses are compared with literature values published for the binary lithium borate glass system.[13] (Unfortunately, no data exist for comparison with the binary Na_2O/B_2O_3 system: $N_2/N_4 = 0$ for all sodium borate glasses within the limited region of glass formation, $R < 0.7$.) Obviously, at any given R value >0.7, the presence of alumina tends to favor nonbridging oxygen formation over tetrahedral boron formation when compared to binary alkali borate glasses. The effect suggests that the $AlO_{4/2}^-$ sites in the framework interact more favorably with the $BO_{2/2}O^-$ units than with the $BO_{4/2}^-$ units.

The second piece of evidence comes from the compositional dependence of the ^{27}Al isotropic chemical shift, depicted in Figure 5. The tendency toward increased deshielding of individual glass framework species with increasing cation content appears to be a general feature and has also been observed for the tetrahedral ^{29}Si and ^{31}P framework species in silicate and phosphate glasses.[50,51] The interpretation of such trends is generally difficult, owing to the complex dependence of isotropic chemical shifts on multiple parameters of structure and bonding. One has to consider two effects, which are probably interrelated: (1) owing to the interaction with the cations, the charges and bond angles associated with the oxygen atoms are modified when the overall cation content is changed, and (2) owing to the network conversion processes, the average connectivity of a specific framework site also changes with cation content. With regard to the latter point, it is interesting to note that, contrary to the ^{29}Si chemical shifts in sodium borosilicate glasses[52] and the ^{31}P chemical shifts in $Al_2O_3-B_2O_3-P_2O_5$ glasses,[38] it is not possible to predict isotropic ^{27}Al chemical shifts consistently by assuming statistical connectivities. This finding indicates a greater degree of intermediate range order around the tetrahedral aluminum sites. Assuming that the $AlO_{4/2}^-$ and $BO_{4/2}^-$ sites are predominantly linked to three-coordinate boron (a contention further supported by ^{11}B−^{27}Al double-resonance experiments discussed in part II of this study), a satisfactory interpretation for the compositional ^{27}Al chemical shift trend can be found: An $AlO_{4/2}^-$ (or $BO_{4/2}^-$) site in a low-sodium glass has a high probability of being coordinated to $BO_{3/2}$ sites (the dominant boron species present here), whereas in high-sodium glasses these tetrahedral sites are more likely to be surrounded by the $BO_{2/2}O^-$ sites mostly present in this compositional region. Figure 12 shows that the corresponding ^{11}B and ^{27}Al isotropic chemical shifts of these tetrahedral species are indeed well-correlated with average three-coordinate boron speciations $N_3/(N_3 + N_2)$ as calculable from the data of Table 2. While this finding is consistent with preferred interactions of three-coordinate boron and tetrahedral

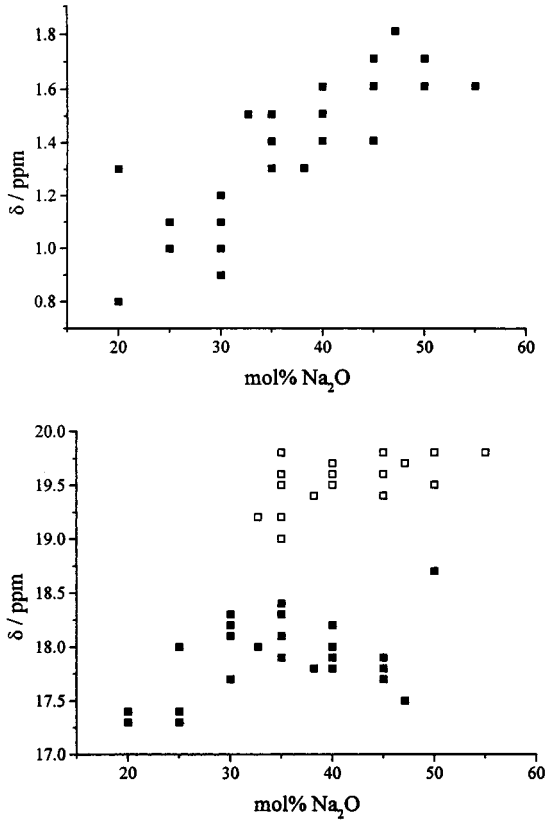

Figure 9. ^{11}B isotropic chemical shifts as a function of sodium oxide concentration. Top: $BO_{4/2}^-$ groups. Bottom: $BO_{2/2}O^-$ groups (open squares), $BO_{3/2}$ groups (filled squares).

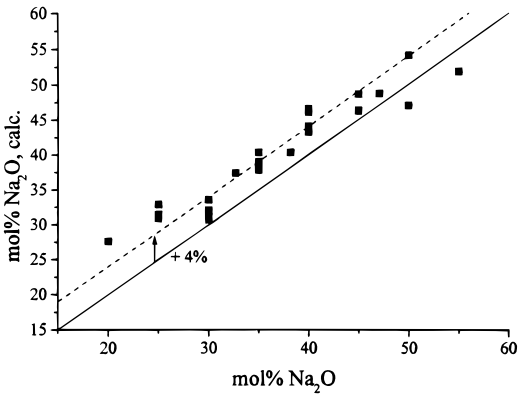

Figure 10. Na_2O content estimated from the boron and aluminum site speciations (vertical axis) versus actual Na_2O content of the glasses. The solid line indicates the identity; the dashed line is a linear fit to the data. For further details, see text.

aluminum species, we emphasize that it does not constitute proof thereof, since the physical basis of the ^{27}Al isotropic chemical shift is not known.

Structural Environment of Sodium. Figure 6 reveals a uniform trend toward more positive ^{23}Na isotropic chemical shifts with increasing sodium content. Analogous trends have been observed in binary sodium borate,[53] silicate,[49,54] and tellurite[55] glasses. In the binary sodium borate glass system, the sodium ions are coordinated by two types of oxygen ions, whose fractional contributions to the cation nearest-neighbor environments change monotonically. As the sodium content is increased, oxygen species bound to trigonal $BO_{3/2}$ units are continuously displaced by oxygen species bound to tetrahedral $BO_{4/2}^-$ units, accounting for the gradual change in the chemical

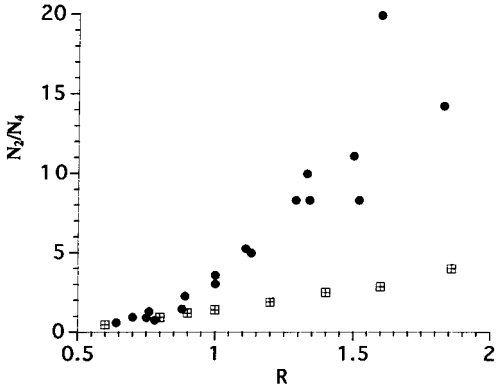

Figure 11. Ratio N_2/N_4 versus R = mol %Na_2O/mol %B_2O_3. Squares, binary lithium borate glasses;[13] filled circles, sodium aluminoborate glasses (this study).

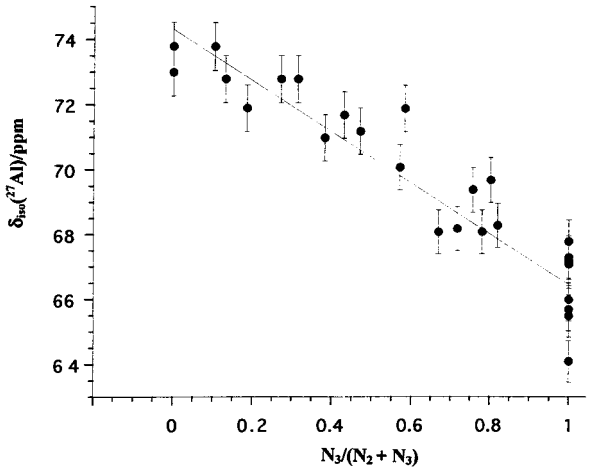

Figure 12. Correlation of the ^{27}Al isotropic chemical shift with the speciation of three-coordinated boron in sodium aluminoborate glasses.

shift. In the sodium aluminoborate glasses, two additional types of oxygen species are present: those that are part of the $AlO_{4/2}^-$ units and nonbridging oxygen from $BO_{2/2}O^-$ sites. Since tetrahedral boron and tetrahedral aluminum sites have identical bond valences, the oxygen atoms associated with both of them are expected to have very similar effects on the ^{23}Na chemical shift. On the other hand, a distinct additional contribution is expected from the nonbridging oxygen atoms associated with the $BO_{2/2}O^-$ sites. Thus, to a first approximation (assuming all aluminum to be four-coordinated), it is reasonable to parametrize the ^{23}Na chemical shift in terms of the structural speciations of the boron and aluminum framework species present where

$$\delta_{iso}(^{23}Na)\ (calcd) = a + b\cdot x_4 + c\cdot x_2 \qquad (3)$$

and

$$x_4 = 2(N_4\cdot \text{mol \% } B_2O_3 + \text{mol \% } Al_2O_3)/(\text{mol \% } B_2O_3 + \text{mol \% } Al_2O_3) \qquad (4)$$

$$x_2 = 2(N_2\cdot \text{mol \% } B_2O_3)/(\text{mol \% } B_2O_3 + \text{mol \% } Al_2O_3) \qquad (5)$$

(For simplicity we neglect here the small amounts of AlO_5 and AlO_6 units in the analysis.) Figure 13 illustrates excellent agreement between calculated and experimental chemical shifts for a curve with parameters a = 14.4 ppm, b = 23.0 ppm, c = 18.0 ppm. It is particularly intriguing that this fit even extends to data of the binary sodium borate glass system.[53] Overall,

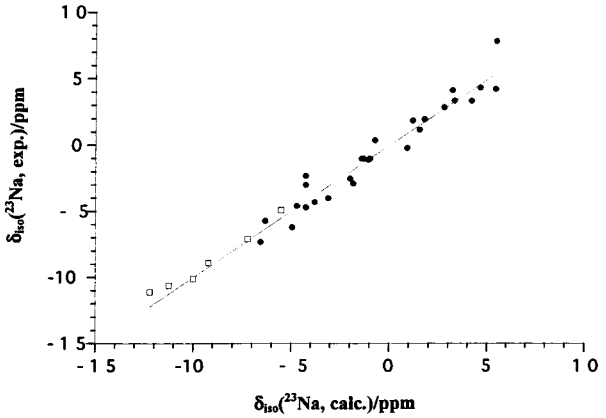

Figure 13. Experimental ^{23}Na isotropic chemical shift versus predicted values from the site speciations via eq 3. Open squares, binary sodium borate glasses;[53] solid circles, sodium aluminoborate glasses (this study).

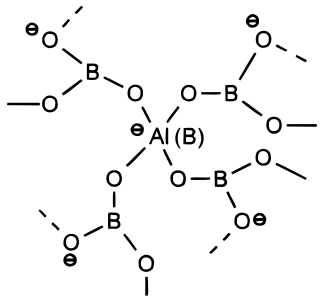

Figure 14. Preferred connectivities in sodium aluminoborate glasses. Tetrahedral $AlO_{4/2}^-$ or $BO_{4/2}^-$ sites are preferentially linked to three-coordinated $BO_{3/2}$ or $BO_{2/2}O^-$ sites.

the ability of predicting the average isotropic sodium NMR shift from the structural speciations of boron and aluminum suggests that the cations are homogeneously distributed within a continuous framework. These data argue strongly against clustering and phase separation models of sodium aluminoborate glasses.

Glass Transition Temperatures and Structure. Numerous attempts have been made to rationalize the physical properties of glasses on the basis of structural considerations.[56−58] Alkali borate systems have been of special interest in this regard, because densities, thermal expansion coefficients, and glass transition temperatures vary nonlinearly with composition.[14−16] For example, in alkali borate glasses T_g initially increases with increasing alkali oxide content, up to a maximum near 27 mol % ($R = 0.37$), and subsequently decreases at higher alkali oxide concentrations. Qualitatively, this effect may be related to the increased connectivity of the borate network, owing to the formation of four-coordinated boron species. On the other hand, a more quantitative understanding is complicated by the fact that the maximum concentration of four-coordinated boron occurs at much higher alkali oxide contents (near 41% ($R = 0.7$)) than the T_g maximum. The discrepancy may be explained as follows:[19] since $BO_{4/2}^-$ units possess a negative formal charge, direct $BO_{4/2}^-$−$BO_{4/2}^-$ links (diborate units) are unfavorable and tend to destabilize the network. Thus, the alkali oxide concentration at which the T_g maximum is observed corresponds to that threshold value of $BO_{4/2}^-$ concentration at which the formation of such diborate units can still be avoided. In a binary alkali borate glass, this theoretical threshold composition is four $BO_{3/2}$ units per three $BO_{4/2}^-$ sites. Assuming quantitative boron conversion this corresponds to a concentration of 30 mol % alkali oxide ($R = 3/7 = 0.428$), which is very close to the value at which the actual T_g maximum is observed. This concept of

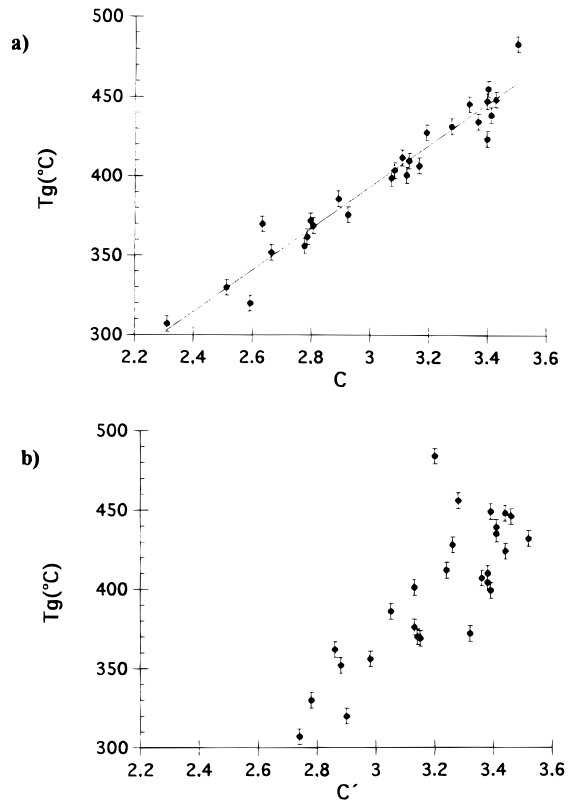

Figure 15. (a) Correlation of the glass transition temperatures with the average connectivity C, calculated and corrected via eq 8. For additional details, see text. (b) Correlation of the glass transition temperatures with the uncorrected average connectivity C. Note that the correlation is much weaker in this case.

an "ideal" concentration of tetrahedral sites can now be applied in conjunction with the structural information from the ^{11}B and ^{27}Al NMR spectra in order to explain the compositional dependence of T_g in sodium aluminoborate glasses. The idea is to have enough bridging oxygen atoms originating from $BO_{3/2}$ or $BO_{2/2}O^-$ groups available to "saturate" the tetrahedral sites with trigonal boron units (see Figure 14). In a glass containing only $BO_{3/2}$ units besides tetrahedral boron and aluminum, the ideal fraction of tetrahedral sites is 0.428 as in binary sodium borate glasses. On the other hand, in a glass containing only $BO_{2/2}O^-$ units (each possessing two bridging oxygen atoms) besides tetrahedral units, this fraction is 0.333. For glasses containing both types of units, the ideal fraction of tetrahedral sites is calculated according to

$$x_4\,(\text{ideal}) = 0.428 - (0.428 - 0.333)\cdot(3 - N_o) \qquad (6)$$

$$N_o = (3x_3 + 2x_2)/(x_3 + x_2) \qquad (7)$$

where N_o defines the average number of bridging oxygen atoms per trigonal boron species. Figure 15a shows a strong correlation of T_g with the average network connectivity computed according to:

$$C = 4x_4^1 + 3x_3 + 2x_2 \qquad (8)$$

In eqs 7 and 8, the quantity x_2 is defined according to eq 5, while x_3 is defined analogously. The quantity x_4^1 is chosen to be the smaller one of the numbers x_4 and x_4(ideal). In an overwhelming number of cases, $x_4 > x_4$(ideal), indicating that some inter-tetrahedral links must be present. As Figure 15b illustrates, the correlation between T_g and C is much weaker if

the experimentally deduced fractions of four-coordinated species are used. This observation suggests that tetrahedral species in excess of the threshold value x_4(ideal) do not contribute to network cohesion and are thus not to be counted in calculating average connectivities. For individual glasses, additional corrections are included accounting for the presence of octahedral Al and three-coordinate boron species having only a single bridging oxygen atom. Despite this success in explaining macroscopic properties on a structural basis, it must be pointed out here that the correlation in Figure 15 does neither include the pure glass former B_2O_3 nor binary sodium borate glasses with low sodium contents. These limitations indicate that mere considerations of network connectivity are insufficient in explaining compositional T_g trends and that contributions from Coulombic interactions must also be taken into account.

Conclusions

Results of a detailed structural study of sodium aluminoborate glasses by high-resolution solid-state ^{11}B,^{23}Na, and ^{27}Al NMR spectroscopies have resulted in quantitative estimates of various framework boron and aluminum structural units as a function of composition. In all of the glasses the overwhelming majority of aluminum species are four-coordinated. To a first approximation, the conversion of aluminum to tetrahedral $AlO_{4/2}^-$ units by the added network modifier Na_2O takes precedence over the boron conversion. Nevertheless, adherence to this model is less strict than previously thought. Considerations of the oxygen balance lead to the conclusion that small amounts of higher-coordinate aluminum species are also present in most of the glasses; further direct (albeit not quantifiable) evidence for these sites is provided by ^{27}Al 3Q-MAS NMR. The ^{23}Na isotropic chemical shifts can be correlated with the structural speciations from ^{11}B and ^{27}Al NMR, reflecting the advent of bridging oxygen atoms linked to tetrahedral species and of nonbridging oxygen atoms, respectively, as the Na_2O contents of the glasses increase. These results are most consistent with a homogeneous distribution of the sodium ions. For the tetrahedral $BO_{4/2}^-$ and $AlO_{4/2}^-$ sites systematic ^{11}B and ^{27}Al chemical shift trends suggest preferential coordination by trigonal boron species. The concept of preferred connectivities is also able to explain compositional trends in the glass transition temperatures. Despite these inferences, more direct evidence for the postulated framework site connectivities is needed. We have recently demonstrated that advanced NMR techniques sensitive to internuclear dipole−dipole couplings can yield much information on this issue.[59] Their detailed application to the present sodium aluminoborate glass system is the subject of part II of this study.

Acknowledgment. We thank Ms. Heike Kamps for the preparation and the thermoanalytical characterization of the glass samples. Valuable discussions with Dr. Leo van Wüllen, Mr. Marko Bertmer, and Professor J. P. Amoureux (Universite des Sciences et Technologies de Lille) are also gratefully acknowledged. J.C.C.C. thanks the Alexander von Humboldt Foundation for a research fellowship. Financial support of this research by the Ministerium für Wissenschaft und Forschung des Landes Nordrhein-Westfalen and by the Fonds der Chemischen Industrie is gratefully appreciated.

References and Notes

(1) DeWaal, H. *Phys. Chem. Glasses* **1962**, *3*, 1.
(2) Owen, A. E. *Phys. Chem. Glasses* **1961**, *2*, 87, 152.
(3) Tuller, H. J.; Button, D. P.; Uhlmann, D. R. *J. Non-cryst. Solids* **1980**, *40*, 93.
(4) Gough, E.; Isard, J. O.; Topping, *J. A. Phys. Chem. Glasses* **1969**, *10*, 89.
(5) Eckert, H. *Prog. Nucl. Magn. Reson. Spectrosc*. **1992**, *24*, 159.
(6) Müller-Warmuth W.; Eckert H. *Phys. Rep*. **1982**, *88*, 91.
(7) Zhong, J.; Bray, P. J. *J. Non-cryst. Solids* **1989**, *67*, 111.
(8) Bray. P. J.; Gravina, S. J.; Hintenlang, D. H.; Mulkern, R. V. *Magn. Reson. Rev.* **1988**, *13*, 263.
(9) Bray, P. J. *J. Non-cryst. Solids* **1987**, *95/96*, 45.
(10) Bray, P. J. *J. Non-cryst. Solids* **1985**, *73*, 19.
(11) Bray, P. J. Geissberger, A. E.; Bucholtz, F.; Harris, I. A. *J. Non-cryst. Solids* **1982**, *52*, 45.
(12) Jellison, Jr., G. E.; Bray, P. J. *J. Non-cryst. Solids* **1978**, *29*, 187.
(13) Yun, Y. H.; Bray, P. J. *J. Non-cryst. Solids* **1981**, *44*, 227.
(14) Shelby, J. E. *J. Am. Ceram. Soc*. **1982**, *66*, 225.
(15) Royle, M.; MacKenzie, J.; Taylor, J.; Sharma, M.; Feller, S. A. *J. Non-cryst. Solids* **1994**, *177*, 242.
(16) Chryssikos, G. D.; Kamitsos, E. I.; Karakassides, M. A. *Phys. Chem. Glasses* **1990**, *31*, 109.
(17) Kamitsos, E. I.; Chryssikos, G. D.; Karakassides, M. A. *Phys. Chem. Glasses* **1988**, *29*, 121.
(18) Chryssikos, G. D.; Kamitsos, E. I.; Yiannopoulos, Y. D. *J. Non-cryst. Solids* **1996**, *196*, 244.
(19) Martin, S. W.; Angell, C. A. *J. Non-cryst. Solids* **1984**, *66*, 429.
(20) Bishop, S. G.; Bray, P. *J. Phys. Chem. Glasses* **1966**, *7*, 73.
(21) Gresch, R.; Müller-Warmuth, W.; Dutz, H. *J. Non-cryst. Solids* **1976**, *21*, 31.
(22) Zhong, J.; Bray, P. J. *J. Non-cryst. Solids* **1986**, *84*, 17.
(23) Araujo, R. J.; Schreurs, J. W. H. *Phys. Chem. Glasses* **1982**, *23*, 185.
(24) Dupree, R.; Holland, D.; Williams, D. S. *Phys. Chem. Glasses* **1985**, *26*, 50.
(25) Bunker, B. C.; Kirkpatrick, R. J.; Brow, R. K.; Turner, G. L.; Nelson, C. *J. Am. Ceram. Soc.* **1991**, *74*, 1430.
(26) Hähnert, M.; Hallas, E. *Rev. Chim. Miner*. **1987**, *24*, 221.
(27) Bunker, B. C.; Kirkpatrick, R. J.; Brow, R. K. *J. Am. Ceram. Soc.* **1991**, *74*, 1425.
(28) For a review, see: Cohen, M. H.; Reif, F. *Solid State Physics*; Seitz, F., Turnbull, D., Eds.; Academic Press: New York, 1957; Vol. 5, p 321.
(29) Samoson, A.; Kundla, E.; Lippmaa, E. *J. Magn. Reson*. **1982**, *49*, 350.
(30) Kriz, H. M.; Bray, P. J. *J. Non-cryst. Solids* **1971**, *6*, 27.
(31) Samoson, A. *Chem. Phys. Lett*. **1985**, *119*, 29.
(32) Lippmaa, E.; Samoson, A.; Mägi, M. *J. Am. Chem. Soc*. **1986**, *108*, 1730.
(33) Jakobsen, H. J.; Skibsted, J.; Bildsoe, H.; Nielsen, N. C. *J. Magn. Reson*. **1989**, *85*, 173.
(34) Jäger, C.; Müller-Warmuth, W.; Mundus, C.; van Wüllen, W. *J. Non-cryst. Solids* **1992,** *149*, 209.
(35) Kunath-Fandrei, G.; Ehrt, D.; Jäger, C. *Z. Naturforsch*. **1995**, *50a*, 413.
(36) Jäger, C. *NMR: Basic Princ. Prog.* **1994**, *31*, 134.
(37) Mundus, C.; Müller-Warmuth, W. *Solid State Nucl. Magn. Reson*. **1995**, *5*, 79.
(38) Buckermann, W. A.; Müller-Warmuth, W.; Mundus, C. *J. Non-cryst. Solids* **1996**, *208*, 217.
(39) Amoureux, J. P. *Solid State Nucl. Magn. Reson*. **1993**, *2*, 83.
(40) Medek, A.; Harwood: J. S.; Frydman, L. *J. Am. Chem. Soc*. **1995**, *117*, 12779.
(41) Fernandez, C.; Amoureux, J. P. *Chem. Phys. Lett*. **1995**, *242*, 449.
(42) Fernandez, C.; Amoureux, J. P. *Solid State Nucl. Magn. Reson*. **1996**, *5*, 315.
(43) Massiot, D.; Touzo, B.; Trumeau, D.; Coutures, J. P.; Virlet, J.; Florian, P.; Grandinetti, P. J. *Solid State Nucl. Magn. Reson.* **1996,** *6*, 73.
(44) Baltisberger, J. H.; Xu, Z.; Stebbins, J. F.; Wang, S. H.; Pines, A. *J. Am. Chem. Soc*. **1996**, *118*, 7209.
(45) Amoureux, J. P.; Fernandez, C.; Steuernagel, S. *J. Magn. Reson.* **1996**, *A123***,** 116.
(46) Ernst, R. R.; Bodenhausen, G.; Wokaun, A. *Principles of Nuclear Magnetic Resonance in One and Two Dimensions*; Oxford University Press: Oxford, U.K., 1987.
(47) Fernandez, C.; Amoureux, J. P.; Chezeau, J. M.; Delmotte, L.; Kessler, H. *Microporous Mater*. **1996**, *6*, 331.
(48) Talyor, T. D.; Rindone, G. E. *J. Am. Ceram. Soc.* **1947**, *53***,** 692.
(49) Brow, R. K.; Kirkpatrick, R. J.; Turner, G. L. *J. Am. Ceram. Soc.* **1990**, *69*, C222.
(50) Dupree, R.; Holland, D.; Williams, D. S. *J. Non-cryst. Solids* **1986**, *81*, 185.
(51) Brow, R. K.; Kirkpatrick, R. J.; Turner, G. L. *J. Non-cryst. Solids* **1990**, *116*, 39.

(52) Van Wüllen, L.; Müller-Warmuth, W.; Papageorgiou, D.; Pentinghaus, H. J. *J. Non-cryst. Solids* **1994**, *171*, 53.
(53) Ratai, E.; Janssen, M.; Eckert, H. *Solid State Ionics* **1998**, *105*, 25.
(54) Gee, B.; Janssen, M.; Eckert, H. *J. Non-cryst. Solids* **1997**, *215*, 41.
(55) Tagg, S. L.; Youngman, R. E.; Zwanziger, J. W. *J. Phys. Chem.* **1995**, *99*, 5111.
(56) Rössler, E.; Kudlik, A.; Hess, K. U.; Dingwell, D. B.; Sokolov, A. P.; Novikov, V. N. *Ber. Bunsen-Ges. Phys. Chem.* **1996**, *100*, 1402.
(57) Ingram, M. D. *Ber. Bunsen-Ges. Phys. Chem.* **1992**, *96*, 1592.
(58) Tatsumisago, M.; Halfpap, B. L.; Green, J. L.; Lindsay, S. M.; Angell, C. A. *Phys. Rev. Lett.* **1990**, *64*, 1549.
(59) Van Wüllen, L.; Züchner, L.; Müller-Warmuth, W.; Eckert, H. *Solid State Nucl. Magn. Reson.* **1996**, *6*, 203.